Inorg. Chem. **2008**, *47*, 855–862

Syntheses, Crystal and Band Structures, and Magnetic and Optical Properties of New $CsLnCdTe_3$ (Ln = La, Pr, Nd, Sm, Gd–Tm, and Lu)

Yi Liu,[†,‡] Ling Chen,[†,§] and Li-Ming Wu,*[,†]

State Key Laboratory of Structural Chemistry, Fujian Institute of Research on the Structure of Matter, Chinese Academy of Sciences, Fuzhou, Fujian 350002, People's Republic of China, Graduate School of the Chinese Academy of Sciences, Beijing 100039, People's Republic of China, and State Key Laboratory of Rare Earth Materials Chemistry and Applications, College of Chemistry and Molecular Engineering, Peking University, Beijing 100871, People's Republic of China

George H. Chan and Richard P. Van Duyne

Department of Chemistry, Northwestern University, 2145 Sheridan Road, Evanston, Illinois 60208-3113

Received August 18, 2007

A series of new quaternary semiconductor materials $CsLnCdTe_3$ (Ln = La, Pr, Nd, Sm, Gd–Tm, and Lu) was obtained from high-temperature solid-state reactions by the reactive halide flux method. These compounds belong to the layered $KZrCuS_3$ structure type and crystallize in the orthorhombic space group *Cmcm* (No. 63). Their structure features two-dimensional $_\infty^2[LnCdTe_3^-]$ layers of edge- and vertex-sharing $LnTe_6$ octahedra with Cd atoms filling the tetrahedral interstices, which stack along *b*-axis. The Cs atoms are located between the $_\infty^2[LnCdTe_3^-]$ layers and are surrounded by eight Te atoms to form a $CsTe_8$ bicapped trigonal prism. Such Te layers are more flexible than the Se analogues in the isostructural $CsLnMSe_3$ to accommodate nearly the entire Ln series. Theoretical studies performed on $CsTmCdTe_3$ show that the material is a direct band gap semiconductor and agrees with the result from a single-crystal optical absorption measurement. Magnetic susceptibility measurements show that the $CsLnCdTe_3$ (Ln = Pr, Nd, Gd, Dy, Tm) materials exhibit temperature-dependent paramagnetism and obey the Curie–Weiss law, whereas $CsSmCdTe_3$ does not.

Introduction

Binary CdTe is an useful material that has been widely studied because of its possible applications as solar cells,[1−8] photovoltaic devices,[9−13] light-emitting diodes,[14−17] semiconductor detectors,[18−21] and thermoelectric materials.[22−25]

* To whom correspondence should be addressed. Tel: (011) 86-591-83705401. E-mail: liming_wu@fjirsm.ac.cn.
† Fujian Institute of Research on the Structure of Matter.
‡ Graduate School of the Chinese Academy of Sciences.
§ Peking University.

(1) Gloeckler, M.; Sites, J. R. *J. Appl. Phys.* **2004**, *95*, 4438.
(2) Karazhanov, S. Z.; Zhang, Y.; Mascarenhas, A.; Deb, S. *J. Appl. Phys.* **2000**, *87*, 8786.
(3) Wendt, R.; Fischer, A.; Grecu, D.; Compaan, A. D. *J. Appl. Phys.* **1998**, *84*, 2920.
(4) Okamoto, T.; Yamada, A.; Konagai, M. *J. Cryst. Growth* **2000**, *214*, 1148.
(5) Bicelli, L. P. *J. Phys. Chem.* **1992**, *96*, 9995.
(6) Youm, I.; Cadene, M.; Candille, M.; Laplaze, D.; Lincot, D. *Phys. Status Solidi A* **1993**, *140*, 471.
(7) Kosyachenko, L. A.; Markov, A. V.; Maslyanchuk, E. L.; Rarenko, I. M.; Sklyarchuk, V. M. *Semiconductors* **2003**, *37*, 1373.
(8) Wu, X. Z. *Sol. Energy* **2004**, *77*, 803.
(9) Emziane, M.; Durose, K.; Halliday, D. P.; Bosio, A.; Romeo, N. *J. Appl. Phys.***2006**, *100*, 013513.
(10) Kosyachenko, L. A.; Mathew, X.; Motushchuk, V. V.; Sklyarchuk, V. M. *Sol. Energy* **2006**, *80*, 148.
(11) Wimbor, M.; Romeo, A.; Igalson, M. *Opto-Electron. Rev.* **2000**, *8*, 375.
(12) Ashokan, R.; Sivananthan, S. *Mater. Sci. Eng., B* **1999**, *67*, 88.
(13) Eggleston, J. M.; Halliday, D. P.; Durose, K. *Compound Semiconductors 1996*; Inst. Phys. Conf. Ser: St Petersburg, Russia, 1996; No. 155, pp 441−444.
(14) Chen, W.; Grouquist, D.; Roark, J. *J. Nanosci. Nanotechnol.* **2002**, *2*, 47.
(15) Gorley, P. M.; Demych, M. V.; Horley, P. P.; Makhniy, V. P.; Ciach, R.; Beltowska-Lehman, E.; Swiatek, Z. *Thin Solid Films* **2002**, *403*, 263.
(16) Sampietro, M.; Ferrari, G.; Bertuccio, G. *J. Appl. Phys.* **2000**, *87*, 7583.
(17) Kosyachenko, L. A.; Maslyanchuk, O. L.; Sklyarchuk, V. M.; Grushko, E. V.; Gnatyuk, V. A.; Aoki, T.; Hatanaka, Y. *J. Appl. Phys.* **2007**, *101*, 013704.

10.1021/ic7016402 CCC: $40.75
Published on Web 01/08/2008

Although CdTe has shown excellent performance as a solar cell material owing to its optimal energy gap, it also has some problems, such as a large absorption coefficient, native defects, electrical contacts, and highly rapid recombination of ions on the surface of CdTe homojunction, that reduce the efficiency of the solar cell.[26−32] To overcome these specific problems, two main approaches have been developed to synthesize desirable semiconductor materials: (1) By synthesizing nanoscale materials, the size of CdTe is reduced (e.g., quantum dots and quantum wells), which results in the change of their chemical and physical properties as compared with the bulk material; some examples include the increase of the band gap energy, the decrease of melting point, and the enhancement of photocatalytic properties.[33−42] This method can alter the energy gap by confining the particle size, which leads to the disruption of the 3D bonding networks in the bulk entity.[43−46] (2) Utilizing the chemical synthesis approaches, many new materials based on CdTe with main-group metals,[44,46−48] transition metals,[49−52] and rare-earth metals[53,54] are designed and can exhibit various structural types and interesting optoelectronic and magnetic properties, which in some cases combine the properties of the corresponding binary phases. The crystal structures and physical properties of these multinary compounds are highly influenced by the presence of metal cations. For example, the alkali metal cations break the 3D condensed CdTe networks into low-dimensional frameworks that may have an impact on their optoelectronic properties,[44,46] the transition metals can be heavily doped in zincblende CdTe to form $Cd_{1-x}M_xTe$ (M = Cr, V, Mn) solid solution and have a remarkable effect on the photoluminescence properties,[49−52] the strong Sm−CdTe interaction leads to photoemission,[53] and the Nd/CdTe heterostructure has a low resistance.[54]

Until now, a large number of multinary transition and alkali metal chalcogenides, formulated as $A_xM_yQ_z$ [44,45,55−61]or $ALnMSe_3$ [62−66](A = alkali metals; Ln = rare earth; M = Mn, Co, Zn, Cd, Hg; Q = chalcogen) and $AYbZnTe_3$ [65] have been discovered. To our knowledge, no quaternary alkali-metal cadmium telluride has been characterized. Only three ternary alkali-metal cadmium tellurides, i.e., $K_2Cd_3Te_4$, $Rb_2Cd_3Te_4$, and $Cs_2Cd_3Te_4$, have been reported,[44,46] and the chemistry of multinary lanthanide cadmium tellurides is rare. Therefore, we attempt to introduce simultaneously both alkali and rare earth metals into the binary CdTe system and anticipate new quaternary compounds. Meanwhile, the band gaps of the target compounds are expected to have a change compared with the 1.44 eV of the bulk CdTe[66] by the additional chemical interactions. The involvement of rare earth elements may also lead to interesting magnetic properties.

In the system of alkali-metal chalcogenide, the inclusion of alkali metals can be prepared by flux methods that are divided into two synthetic pathways. One is the molten alkali-metal polychalcogenide flux method, and the other is reactive

(18) Niraula, M.; Nakamura, A.; Aoki, T.; Tomita, Y.; Hatanaka, Y. *Phys. Status Solidi B* **2002**, *229*, 1103.
(19) Veger, L.; Bonnefoy, J. P.; Glasser, F.; OuvrierBuffet, P. *J. Electron. Mater.* **1997**, *26*, 738.
(20) Niraula, M.; Mochizuki, D.; Aoki, T.; Tomita, Y.; Hatanaka, Y. *J. Cryst. Growth* **2000**, *214*, 1116.
(21) Okada, K.; Sakurai, Y.; Suematsu, H. *Appl. Phys. Lett.* **2007**, *90*, 063504.
(22) Cho, S.; DiVenere, A.; Wong, G. K.; Ketterson, J. B.; Meyer, J. R.; Hoffman, C. A. *Solid State Commun.* **1997**, *102*, 673.
(23) Paez, B. A. *Phys. Status Solidi B* **2000**, *220*, 221.
(24) Soundararajan, R.; Lynn, K. G.; Awadallah, S.; Szeles, C.; Wei, S. H. *J. Electron. Mater.* **2006**, *35*, 1333.
(25) Vurgaftman, I.; Meyer, J. R.; Hoffman, C. A.; Cho, S.; DiVenere, A.; Wong, G. K.; Ketterson, J. B. *J. Phys.: Condens. Matter* **1999**, *11*, 5157.
(26) Berding, M. A. *Phys. Rev. B* **1999**, *60*, 8943.
(27) Savitsky, A.; Parfenyuk, O.; Ilashchuk, M.; Fochouk, P.; Burachek, V. *J. Cryst. Growth* **1998**, *185*, 1155.
(28) Dharmadasa, I. M. *Prog. Cryst. Growth Charact. Mater.* **1998**, *36*, 249.
(29) Cohen, R.; Lyahovitskaya, V.; Poles, E.; Liu, A.; Rosenwaks, Y. *Appl. Phys. Lett.* **1998**, *73*, 1400.
(30) Romero, M. J.; Gessert, T. A.; Al-Jassim, M. M. *Appl. Phys. Lett.* **2002**, *81*, 3161.
(31) Protasenko, V.; Bacinello, D.; Kuno, M. *J. Phys. Chem. B* **2006**, *110*, 25322.
(32) Bangert, E.; Boege, P.; Latussek, V.; Landwehr, G. *Semicond. Sci. Technol.* **1993**, *8*, S99.
(33) Bao, J. M.; Bragas, A. V.; Furdyna, J. K.; Merlin, R. *Solid State Commun.* **2003**, *127*, 771.
(34) Brunhes, T.; Andre, R.; Arnoult, A.; Cibert, J.; Wasiela, A. *Phys. Rev. B* **1999**, *60*, 11568.
(35) Bruchhausen, A.; Fainstein, A.; Jusserand, B.; Andre, R. *Phys. Rev. B* **2006**, *73*, 085305.
(36) Besombes, L.; Marsal, L.; Kheng, K.; Mariette, H. *Phys. Status Solidi B* **2001**, *224*, 621.
(37) Jeukens, C. R. L. P. N.; Christianen, P. C. M.; Maan, J. C.; Yakovlev, D. R.; Ossau, W.; Wojtowicz, T.; Karczewski, G.; Kossut, J. *Phys. Status Solidi A* **2002**, *190*, 813.
(38) Peng, Z. A.; Peng, X. G. *J. Am. Chem. Soc.* **2001**, *123*, 183.
(39) Bailey, R. E.; Nie, S. M. *J. Am. Chem. Soc.* **2003**, *125*, 7100.
(40) Redlinski, P. *J. Appl. Phys.* **2006**, *99*, 063702.
(41) Terai, Y.; Kuroda, S.; Takita, K.; Okuno, T.; Masumoto, Y. *Appl. Phys. Lett.* **1998**, *73*, 3757.
(42) Karczewski, G.; Mackowski, S.; Kutrowski, M.; Wojtowicz, T.; Kossut, J. *Appl. Phys. Lett.* **1999**, *74*, 3011.
(43) Murray, C. B.; Norris, D. J.; Bawendi, M. G. *J. Am. Chem. Soc.* **1993**, *115*, 8706.
(44) Axtell, E. A.; Liao, J. H.; Pikramenou, Z.; Kanatzidis, M. G. *Chem. Eur. J.* **1996**, *2*, 656.
(45) Axtell, E. A.; Liao, J. H.; Pikramenou, Z.; Park, Y. B.; Kanatzidis, M. G. *J. Am. Chem. Soc.* **1993**, *115*, 12191.
(46) Narducci, A. A.; Ibers, J. A. *J. Alloys Compds.* **2000**, *306*, 170.
(47) Saucedo, E.; Fornaro, L.; Sochinskii, N. V.; Cuna, A.; Corregidor, V.; Granados, D.; Diequez, E. *IEEE Trans. Nucl. Sci.* **2004**, *51*, 3105.
(48) Wang, Y. C.; DiSalvo, F. J. *J. Solid State Chem.* **1999**, *148*, 464.
(49) Xie, W. H.; Liu, B. G. *J. Appl. Phys.* **2004**, *96*, 3559.
(50) Kreissl, J.; Schulz, H. J. *J. Cryst. Growth* **1996**, *161*, 239.
(51) Aoudia, A.; Rzepka, E.; Lusson, A.; Tromsoncarli, A.; Schneider, D.; Marfaing, Y.; Triboulet, R. *Opt. Mater.* **1995**, *4*, 241.
(52) Udo, M. K.; Villeret, M.; Miotkowski, I.; Mayur, A. J.; Ramdas, A. K.; Rodriguez, S. *Phys. Rev. B* **1992**, *46*, 7459.
(53) Guziewicz, E.; Kowalski, B. J.; Orlowski, B. A.; Johnson, R. L. *Surf. Sci.* **2001**, *482*, 512.
(54) Brun-Le Cunff, D.; Daudin, B. *J. Appl. Phys.* **1996**, *79*, 8541.
(55) Klepp, K. O.; Bronger, W. *Rev. Chim. Miner.* **1983**, *20*, 682.
(56) Axtell, E. A.; Kanatzidis, M. G. *Chem. Mater.* **1996**, *8*, 1350.
(57) Klepp, K. O. *J. Alloys Compds.* **1992**, *182*, 281.
(58) Klepp, K. O.; Prager, K. *Z. Naturforsch., B: Chem. Sci.* **1992**, *47*, 491.
(59) Sommer, H.; Hoppe, R.; Jansen, M. *Naturwissenschaften* **1976**, *63*, 194.
(60) Li, J.; Chen, Z.; Lam, K. C.; Mulley, S.; Proserpio, D. M. *Inorg. Chem.* **1997**, *36*, 684.
(61) Chen, X. A.; Huang, X. Y.; Li, J. *Inorg. Chem.* **2001**, *40*, 1341.
(62) Chan, G. H.; Sherry, L. J.; Van Duyne, R. P.; Ibers, J. A. *Z. Anorg. Allg. Chem.* **2007**, *633*, 1343.
(63) Huang, F. Q.; Mitchell, K.; Ibers, J. A. *Inorg. Chem.* **2001**, *40*, 5123.
(64) Mitchell, K.; Haynes, C. L.; McFarland, A. D.; Van Duyne, R. P.; Ibers, J. A. *Inorg. Chem.* **2002**, *41*, 1199.
(65) Mitchell, K.; Huang, F. Q.; Caspi, E. N.; McFarland, A. D.; Haynes, C. L.; Somers, R. C.; Jorgensen, J. D.; Van, Duyne, R. P.; Ibers, J. A. *Inorg. Chem.* **2004**, *43*, 1082.
(66) Mitchell, K.; Huang, F. Q.; McFarland, A. D.; Haynes, C. L.; Somers, R. C.; Van Duyne, R. P.; Ibers, J. A. *Inorg. Chem.* **2003**, *42*, 4109.

alkali halide flux method. The former has proven to be an effective method for the synthesis of a lot of low-dimensional phases with interesting structures over the past decade.[44,62−72] The alkali-metal polychalcogenide flux method is dangerous and inconvenient, because it requires the stoichiometric reactions of elemental alkali and chalcogen in liquid ammonia, a process that often leads to a mixture of products,[73] whereas the reactive halide flux method overcomes the defects and has successfully produced many interesting solid-state chalcogenide materials.[74−80] A limitation of the reactive halide flux method is the difficulty of synthesizing metal polytellurides with long terminal or bridging units as building blocks.

By employing the reactive halide flux method, we have successfully synthesized a series of $CsLnCdTe_3$ (Ln = La, Pr, Nd, Sm, Gd−Tm, and Lu) that adopt the layered $KZrCuS_3$ [81] structure type. In this paper, we present the synthesis, crystal structures, magnetic and optical properties, and electronic structure studies of these new compounds.

Experimental Section

Syntheses. The following reactants were used as purchased and stored in a glovebox filled with purified N_2 (moisture and oxygen level is less than 0.1 ppm) to reduce contamination, and all manipulations were performed inside the glovebox. Rare earth elements were purchased from Huhhot Jinrui Rare Earth Co., Ltd.: La (99.99%), Pr (99.5%), Nd (99.9%), Sm (99.9%), Gd (99.95%), Tb (99.95%), Dy (99.95%), Ho (99.95%), Er (99.95%), Tm (99.95%), Lu (99.95%). Cd (99.95%) and Te (99.99%) were purchased from Alfa Aesar China (Tianjin) Co., Ltd. CsCl (99.5%) was purchased from XinJiang Research Institute of Non-Ferrous Metals. The $CsLnCdTe_3$ compounds were produced by the mixture of 1.0 mmol of Ln, 0.5 mmol of Cd, 2.0 mmol of Te, and 1.2 mmol (200 mg) of CsCl via the high-temperature solid-state reaction. CsCl worked as a flux to assist the crystallization of the target compounds and also as a cesium source in these reactions. Typically, a mixture of the reagents was loaded into a short fused silica tube, which was subsequently situated inside a larger evacuated quartz tube (10 mm i.d.). The tube was flame-sealed under a 10^{-3} Pa atmosphere and then placed into a temperature-controlled furnace. The heating and cooling profiles for all samples are as followed. The furnace was ramped to 850 °C at a rate of 30 °C/h, the temperature was held constant at 850 °C for 96 h and then slowly cooled at 3 °C /h to 200 °C before the furnace was turned off, and then the samples were cooled radiatively to ambient temperature in the furnace. The raw products were washed first with distilled water to remove excess flux and the chloride byproducts and dried with ethanol. The cleaned products are X-ray pure; such purity has also been supported by the magnetic measurement, with only one exception: $CsLuCdTe_3$ is mixed with two other minor phases, elemental Te and binary CdTe, as indicated by the X-ray analysis. No Eu and Yb compounds could be synthesized. All these compounds crystallize as dark-red blocks or plates, and their surfaces turn black after a few hours of exposure in air, except that of $CsTmCdTe_3$.

Microprobe elemental analyses were performed on several single crystals of the $CsLnCdTe_3$ compounds, including the crystals used for X-ray diffraction analysis. Spectra were collected on a field-emission scanning electron microscope (FESEM, JSM6700F) equipped with an energy dispersive X-ray spectroscope (EDX, Oxford INCA). The results indicate the presence of Cs, Ln, Cd, and Te in the approximate molar ratio 1.00:1.08:1.14:3.22 within the limitations of this technique, and no Cl from the flux or Si or O from the quartz tube was detected. The exact composition was established from the X-ray structure determination. The phase identity and purity were examined by the powder X-ray diffraction analysis, and each experimental powder pattern matches well with the simulated powder pattern.

Single-Crystal Structure Determination. The single crystals are selected from the products and sealed inside a 0.3 mm i.d. thin-walled glass capillary inside an argon-filled glovebox with moisture level below 0.1 ppm. Diffraction data were collected on either a Rigaku Mercury CCD diffractometer or a Rigaku Saturn70 CCD diffractometer equipped with graphite-monochromated Mo Kα radiation (λ = 0.71073 Å) at room temperature. The data were corrected for the Lorentz factor, polarization, air absorption, and absorption due to the variations in the path length through the detector faceplate. The absorption correction based on the multiscan method was also applied.[82] The structures were solved by the direct methods and refined by the full-matrix least-squares fitting on F^2 in orthorhombic *Cmcm* space group with the aid of the SHELX-97 software package.[83] All of the atoms were refined with the anisotropic displacement parameters and a secondary extinction correction. Crystallographic data and structural refinements for the compounds are summarized in Table 1. Table 2 presents the selected bond distances for $CsLnCdTe_3$ (Ln = La, Pr, Nd, Sm, Gd−Tm, and Lu). More details on the crystallographic studies, as well as atom displacement parameters, are available in the Supporting Information.

Magnetic Susceptibility Measurements. The dc magnetic susceptibility measurements were made on a PPMS-9T magnetometer at temperatures between 2.0 and 300 K. The polycrystalline sample of $CsLnCdTe_3$ (Ln = Pr, Nd, Sm, Gd, Dy, Tm) was ground to a fine powder to minimize possible anisotropic effects and loaded into a gelatin capsule. The sample was cooled in a constant magnetic field of 5000 Oe for measurements of magnetization versus temperature. The susceptibility data were collected every 0.5 K between 2 and 10 K, every 1.0 K between 10 and 20 K, every 2.0 K between 20 and 100 K, and then every 5.0 K in the higher temperature range. For all compounds, corrections were made for the susceptibility of the container and the ion core diamagnetism.

(67) Hess, R. F.; Gordon, P. L.; Tait, C. D.; Abney, K. D.; Dorhout, P. K. *J. Am. Chem. Soc.* **2002**, *124*, 1327.
(68) Kanatzidis, M. G. *Chem. Mater.* **1990**, *2*, 353.
(69) Kim, J. H.; Chung, D. Y.; Kanatzidis, M. G. *Chem. Commun.* **2006**, 1628.
(70) Martin, B. R.; Dorhout, P. K. *Inorg. Chem.* **2004**, *43*, 385.
(71) Pell, M. A.; Ibers, J. A. *J. Am. Chem. Soc.* **1995**, *117*, 6284.
(72) Pell, M. A.; Ibers, J. A. *Chem. Mater.* **1996**, *8*, 1386.
(73) Smith, D. M.; Ibers, J. A. *Coord. Chem. Rev.* **2000**, *200*, 187.
(74) Yao, J. Y.; Deng, B.; Sherry, L. J.; McFarland, A. D.; Ellis, D. E.; Van Duyne, R. P.; Ibers, J. A. *Inorg. Chem.* **2004**, *43*, 7735.
(75) Huang, F. Q.; Ibers, J. A. *J. Solid State Chem.* **2001**, *160*, 409.
(76) Huang, F. Q.; Choe, W.; Lee, S.; Chu, J. S. *Chem. Mater.* **1998**, *10*, 1320.
(77) Bucher, C. K.; Hwu, S. J. *Inorg. Chem.* **1994**, *33*, 5831.
(78) Kim, S. J.; Park, S. J.; Yun, H. S.; Do, J. W. *Inorg. Chem.* **1996**, *35*, 5283.
(79) Zeng, H. Y.; Mattausch, H.; Simon, A.; Zheng, F. K.; Dong, Z. C.; Guo, G. C.; Huang, J. S. *Inorg. Chem.* **2006**, *45*, 7943.
(80) Folchnandt, M.; Schleid, T. *Z. Anorg. Allg. Chem.* **1998**, *624*, 1595.
(81) Mansuetto, M. F.; Keane, P. M.; Ibers, J. A. *J. Solid State Chem.* **1992**, *101*, 257.
(82) CrystalClear, version 1.3.5; Rigaku Corp.: Woodlands, TX, 1999.
(83) Sheldrick, G. M. *SHELXTL, Crystallographic Software Package*, version 5.1; Bruker-AXS: Madison, WI, 1998.

Table 1. Crystal Data and Structure Refinements for $CsLnCdTe_3$ (Ln = La, Pr, Nd, Sm, Gd−Tm, and Lu)[a]

	$CsLaCdTe_3$	$CsPrCdTe_3$	$CsNdCdTe_3$	$CsSmCdTe_3$	$CsGdCdTe_3$
fw	767.02	769.02	772.35	778.46	785.36
a (Å)	4.6392(17)	4.594(3)	4.5730(4)	4.5472(6)	4.5122(17)
b (Å)	16.702(7)	16.770(12)	16.7501(15)	16.804(2)	16.783(7)
c (Å)	12.168(5)	12.023(9)	11.9675(10)	11.8947(18)	11.818(5)
V (Å^3)	942.8(6)	926.2(11)	916.69(14)	908.9(2)	894.9(6)
D_{cal} (g/cm^3)	5.404	5.515	5.596	5.689	5.829
μ (cm^{-1})	195.33	205.30	210.93	220.23	232.16
R_1 [b]	0.0164	0.0327	0.0256	0.0256	0.0319
wR_2 [c]	0.0581	0.0907	0.0534	0.0509	0.0783

	$CsTbCdTe_3$	$CsDyCdTe_3$	$CsHoCdTe_3$	$CsErCdTe_3$	$CsTmCdTe_3$	$CsLuCdTe_3$
fw	787.03	790.61	793.04	795.37	797.04	803.08
a (Å)	4.4956(4)	4.483(7)	4.4727(15)	4.4627(14)	4.457(2)	4.444(4)
b (Å)	16.7790(16)	16.75(3)	16.802(6)	16.812(6)	16.824(8)	16.841(17)
c (Å)	11.7804(11)	11.745(18)	11.727(4)	11.706(4)	11.696(6)	11.672(11)
V (Å^3)	888.62(14)	882(2)	881.3(5)	878.2(5)	877.1(7)	873.6(15)
D_{cal} (g/cm^3)	5.883	5.956	5.977	6.016	6.036	6.106
μ (cm^{-1})	238.75	245.14	250.27	256.61	262.41	274.90
R_1 [b]	0.0284	0.0581	0.0329	0.0247	0.0207	0.0487
wR_2 [c]	0.0701	0.1484	0.0830	0.0585	0.0491	0.1462

[a] For all structures, $Z = 4$, space group = *Cmcm*, T =293(2) K, and $\lambda = 0.710\ 73$ Å. [b] $R_1 = \sum||F_o| - |F_c||/\sum|F_o|$. [c] $wR_2 = [\sum w(F_o^2 - F_c^2)^2/\sum w(F_o^2)^2]^{1/2}$

Table 2. Selected Bond Lengths (Å) for $CsLnCdTe_3$ (Ln = La, Pr, Nd, Sm, Gd−Tm, and Lu)

	$CsLaCdTe_3$	$CsPrCdTe_3$	$CsNdCdTe_3$	$CsSmCdTe_3$	$CsGdCdTe_3$
Cs−Te1 × 4	3.9250(11)	3.9328(19)	3.9280(6)	3.9343(7)	3.9262(13)
Cs−Te1 × 2	4.2010(15)	4.149(3)	4.1284(7)	4.1048(9)	4.0741(17)
Cs−Te2 × 2	3.8138(15)	3.815(2)	3.8119(9)	3.8178(10)	3.8125(18)
Ln−Te1 × 4	3.2307(9)	3.1918(16)	3.1749(4)	3.1532(5)	3.1300(10)
Ln−Te2 × 2	3.2266(11)	3.195(2)	3.1804(4)	3.1653(5)	3.1442(12)
Cd−Te1 × 2	2.7930(11)	2.7949(19)	2.7877(7)	2.7880(8)	2.7797(14)
Cd−Te2 × 2	2.8989(11)	2.8834(19)	2.8744(8)	2.8707(8)	2.8566(14)

	$CsTbCdTe_3$	$CsDyCdTe_3$	$CsHoCdTe_3$	$CsErCdTe_3$	$CsTmCdTe_3$	$CsLuCdTe_3$
Cs−Te1 × 4	3.9268(8)	3.923(4)	3.9314(12)	3.9328(11)	3.9389(12)	3.944(3)
Cs−Te1 × 2	4.0625(9)	4.047(5)	4.0444(15)	4.0377(13)	4.0346(16)	4.028(3)
Cs−Te2 × 2	3.8133(11)	3.810(5)	3.8145(17)	3.8183(14)	3.8204(16)	3.829(3)
Ln−Te1 × 4	3.1136(5)	3.101(4)	3.0948(9)	3.0866(8)	3.0792(11)	3.066(2)
Ln−Te2 × 2	3.1350(4)	3.126(4)	3.1220(11)	3.1160(10)	3.1141(13)	3.106(3)
Cd−Te1 × 2	2.7780(9)	2.776(4)	2.7743(13)	2.7728(11)	2.7743(12)	2.773(3)
Cd−Te2 × 2	2.8495(9)	2.845(4)	2.8438(13)	2.8404(11)	2.8397(12)	2.833(3)

Optical Microspectroscopy Measurements. Single-crystal absorption measurements on $CsTmCdTe_3$ in the range 400 nm (3.10 eV) to 800 nm (1.55 eV) at 293 K were performed with the use of a Nikon TE300 inverted microscope coupled by a fiber optic to an Ocean Optics model S2000 spectrometer. The spectrometer was fiber optically coupled to a Nikon TE300 inverted microscope with its IR filter removed. The single crystal was positioned at the focal point above a 20× objective with the use of a goniometer mounted on translation stages (Line Tool Co.). Fine alignment of the microscope assembly was achieved by maximizing the transmission of the lamp profile. White light originated from the TE300 tungsten−halogen lamp passed through a polarizer before impinging on the crystal, and the transmitted light was then spatially filtered before being focused into the 400 μm core diameter fiber coupled to the spectrometer. The optical band gaps were determined from the absorbance versus energy data via a linear regression method.

Theoretical Calculations. The crystallographic data of $CsTmCdTe_3$ were employed for theoretical calculations of the electronic band structure. The electronic configurations for Cs, Tm, Cd and Te are as follows: Cs, $[Xe]6s^1$; Tm, $[Xe]4f^{12}5d^16s^2$; Cd, $[Kr]4d^{10}5s^2$; and Te, $[Kr]4d^{10}5s^25p^4$. Relativistic effects are taken into account within the scalar−relativistic approximation. The calculations for the present compound were treated with the highly accurate full-potential linear augmented plane wave plus local orbital (FP-LAPW+LO) method within density-functional theory (DFT),[84−86] implemented in the WIEN2K program package.[87] The Perdew−Burke−Ernzerhof generalized gradient approximation with a Hubbard U correction (GGA(PBE)+U) for the exchange-correlation potentials were used in the calculations.[88,89] This approach corrects the strong Coulomb correlation effects associated with partially filled f levels. The Hubbard parameter U reflects the strength of the on-site Coulomb interaction, and the parameter J, adjusts the strength of the exchange interaction. In the somewhat simplified, yet rotationally invariant, method by Dudarev et al.,[90] these two parameters are combined into a single parameter, $U_{eff} = U - J$.

(84) Yu, R.; Krakauer, H.; Singh, D. *Phys. Rev. B* **1991**, *43*, 6411.
(85) Wimmer, E.; Krakauer, H.; Weinert, M.; Freeman, A. J. *Phys. Rev. B* **1981**, *24*, 864.
(86) Mattheiss, L. F.; Hamann, D. R. *Phys. Rev. B* **1986**, *33*, 823.
(87) Blaha, P.; Schwarz, K.; Madsen, G. K.; Kvasnicka, D.; Luitz, J. *WIEN2k. An Augmented Plane Wave + Local Orbitals Program for Calculating Crystal Properties*; Techn. Universität Wien: Vienna, Austria, 2001.
(88) (a) Ong, K. P.; Bai, K.; Blaha, P.; Wu, P. *Chem. Mater.* **2007**, *19*, 634. (b) Hinuma, Y.; Meng, Y. S.; Kang, K. S.; Ceder, G. *Chem. Mater.* **2007**, *19*, 1790.
(89) (a) Etz, C.; Stoeffler, D. *Eur. Phys. J. B.* **2006**, *54*, 429. (b) Mestnik, J.; Pereira, L. F. D.; Lalic, M. V.; Carbonari, A. W. *Physica B* **2007**, *389*, 73.
(90) Dudarev, S. L.; Botton, G. A.; Savrasov, S. Y.; Humphreys, C. J.; Sutton, A. P. *Phys. Rev. B* **1998**, *57*, 1505.

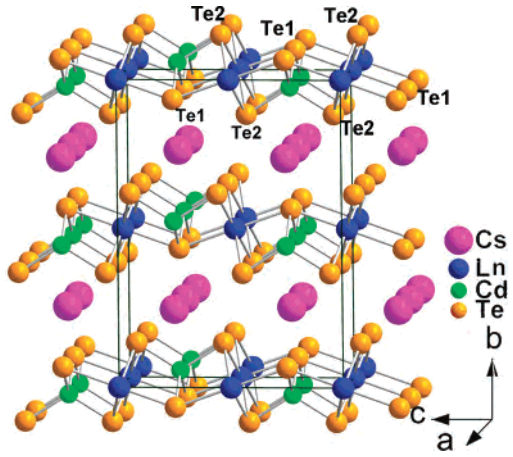

Figure 1. View of $CsLnCdTe_3$ projected slightly off the *a*-axis.

As expected, $CsTmCdTe_3$ is sensitive to the choice of the U_{eff} value. Consequently, after comparing the computational results with the different values of U_{eff}, an optimum value of U_{eff} = 1.30 Ry is suggested for the GGA(PBE)+U scheme. The muffin-tin (MT) radii (bohr) were set to be 2.5 for Cs, 2.5 for Tm, 2.5 for Cd, and 2.45 for Te. The value of RKMAX (smallest muffin tin radius multiplied by the maximum *k* value in the expansion of plane waves in the basis set) determines the accuracy of the basis set, and RKMAX = 7 is used in this study. The densities and potentials (GMAX) is set to 14. The *k* integration over the Brillouin zone is performed with an 8 × 8 × 3 Monkhorst−Pack mesh and the cutoff energy between valence and core states is −6.0 Ry. The density-of-states (DOS) is calculated with the modified tetrahedron method.[91] The self-consistent calculations are considered to have converged only when the calculated total energy of the crystal is less than 0.0001 Ry.

Results and Discussion

Syntheses and Structure. These 11 isostructural compounds $CsLnCdTe_3$ (Ln = La, Pr, Nd, Sm, Gd−Tm and Lu) with the space group *Cmcm* were obtained via the reactive CsCl flux method at 850 °C; however, an attempt to synthesize $CsLnCdTe_3$ (Ln = Eu, Yb) was unsuccessful. For the Eu analogue, it is known that Eu prefers to be in a formal oxidation state of 2+ rather than 3+ in some chalcogenide systems,[92−94] whereas for the Yb analogue, it is unknown why the compound could not be synthesized. Generally, the pure target compounds are available after washing, and only for the Lu analogue is there always a mixture of minor phases of the element Te and binary CdTe.

These $CsLnCdTe_3$ compounds belong to the layered $KZrCuS_3$ structure type.[81] The main structural motifs are the $^2_\infty[LnCdTe_3^-]$ layers parallel to the *ac*-plane and the Cs^+ cations surrounded by eight Te anions located between such layers (Figures 1 and 2). The three building units are identified as $LnTe_6$ octahedron, $CdTe_4$ tetrahedron, and $CsTe_8$ bicapped trigonal prism. The $^2_\infty[LnCdTe_3^-]$ layers are constructed from a slightly distorted $LnTe_6$ octahedron via edge-sharing with two neighboring $LnTe_6$ octahedra along the *a*-axis and vertex-sharing with two other $LnTe_6$ octahedra along the *c*-direction, and the thus-formed distorted tetrahedral interstices are occupied by the Cd atoms (Figure 2). Between the neighboring $^2_\infty[LnCdTe_3^-]$ layers, Cs^+ cations are surrounded by eight Te atoms in a bicapped trigonal prismatic geometry (Figure 3). Because there is no Te−Te bond in $CsLnCdTe_3$, the formal oxidation states of A/Ln/Cd/Te can be assigned as 1+/3+/2+/2−, respectively. It was found in $CsLnMSe_3$ compounds that the smaller Zn atom crystallizes the heavier lanthanides Ln = Gd−Yb, while the larger Cd/Hg atom prefers the lighter lanthanides Ln = La−Nd;[66] the reason is presumed to be the size-matching in order to maintain the stability of the anionic framework of edge-sharing MSe_4 tetrahedra and $LnSe_6$ octahedra. Comparably, in the title compounds reported here, the Te-containing layers are more accommodating than the Se-containing layers. For example, the bond angles around the central Cd atom of $CdSe_4$ tetrahedron are much more deviated from the ideal tetrahedral angles than those of $CdTe_4$. The $CdSe_4$ tetrahedron is more elongated than the $CdTe_4$ tetrahedron; such distortion may narrow the range of lanthanides to form the

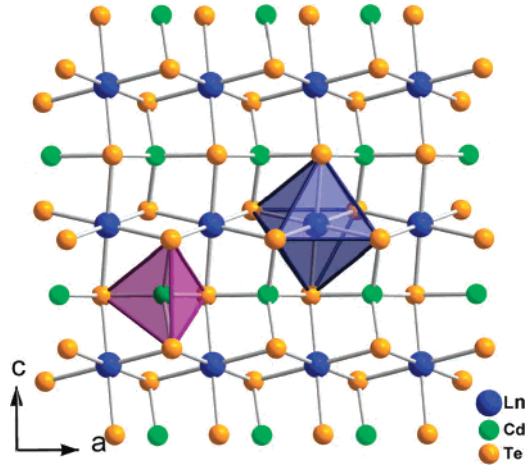

Figure 2. View of the $^2_\infty[LnCdTe_3^-]$ layer shown approximately along the *b*-axis ($LnTe_6$ octahedron and $CdTe_4$ tetrahedron are shaded in light blue and purple, respectively).

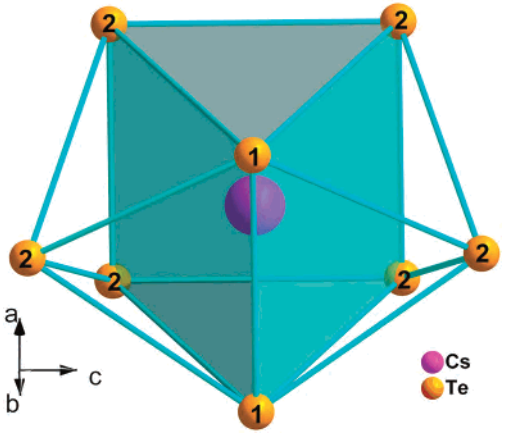

Figure 3. The $CsTe_8$ bicapped trigonal prism shown approximately down the *b*-axis.

(91) Blochl, P. E.; Jepsen, O.; Andersen, O. K. *Phys. Rev. B* **1994**, *49*, 16223.
(92) Aitken, J. A.; Larson, P.; Mahanti, S. D.; Kanatzidis, M. G. *Chem. Mater.* **2001**, *13*, 4714.
(93) Evenson, C. R.; Dorhout, P. K. *Inorg. Chem.* **2001**, *40*, 2875.
(94) Knaust, J. M.; Polyakova, L. A.; Dorhout, P. K. *Z. Kristallogr.—New Cryst. Struct.* **2005**, *220*, 295.

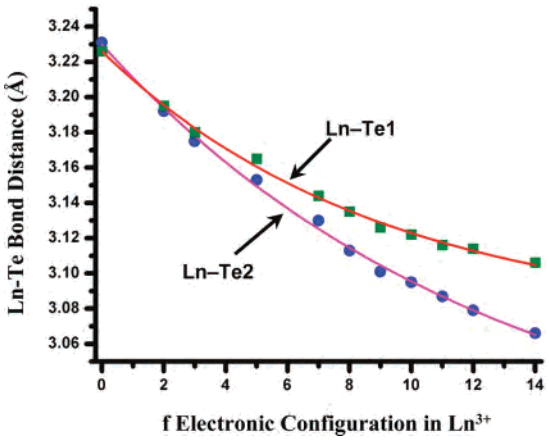

Figure 4. Plots of Ln−Te bond distance vs f electronic configuration for $CsLnCdTe_3$ and the relative best fit parabola.

Se-containing compounds. As a result, the present $CsLnCdTe_3$ compounds have been crystallized over nearly the entire range of lanthanides.

In the $CsLnCdTe_3$ compounds (Table 2), the Ln−Te distances range from 3.066(2) to 3.2307(9) Å, which are consistent with the previously reported distances of 3.0296(7)−3.3585(5) Å in, for example, $CsLnZnTe_3$, $LnCu_{(0.32-0.40)}Te_2$, $SmTe_3$, $Er_7Ni_2Te_2$, or $Lu_7Z_2Te_2$ (Z = Ni, Pd, Ru).[74,95−98] The Cd−Te distances vary from 2.773(3) to 2.8989(11) Å and agree with those [2.770(6)−2.931(3) Å] in $K_2Cd_3Te_4$ and $Cs_2Cd_3Te_4$.[44,46] The Cs−Te distances ranging from 3.810(5) to 4.2010(15) Å are comparable to those in $Cs_2Cd_3Te_4$ [3.883(1)−4.003(1) Å] and $CsLnZnTe_3$ [3.7933(8)−4.2665(6) Å][46,74] and show typical ionic bonding. The lanthanide contraction has also been observed here. As shown in Figure 4, the bond distances of Ln−Te1 and Ln−Te2 show monotonic shrinking with an increase of 4f electrons in the Ln^{3+} ion. As a result, both the *a*- and *c*-axes, which are parallel to the $_\infty^2[LnCdTe_3^-]$ layer, are shortened; however, the *b*-axis, which is perpendicular to the layer, has no distinct tendency to change (Table 1). The lanthanide contraction is expressed by a quadratic equation, $d(\text{Ln}-\text{X}) = A_0 - A_1n + A_2n^2$, where A_0 is a constant, A_1 and A_2 are linear and quadratic optimized parameters of the regression, and $0 \le n \le 14$ is the number of 4f electrons in the Ln^{3+} ion.[99] The polynomial fit over the experimental data (Ln−Te1 and Ln−Te2), gives A_0, A_1, A_2, and R^2 (the correlation factor) of 3.23, 1.78×10^{-2}, 4.49×10^{-4}, and 99.7% for the former and 3.22, 1.48×10^{-2}, 4.61×10^{-4}, and 99.7% for the latter, which show that the lanthanide contraction trend adapts well to an quadratic equation expression.

Magnetic Properties. Magnetic properties for $CsLnCdTe_3$ (Ln = Pr, Nd, Sm, Gd, Dy, Tm) have been studied at an applied field of 5000 Oe in the temperature range of 2−300 K. Except for $CsPrCdTe_3$ and $CsSmCdTe_3$, they are paramagnetic over the entire experimental temperature range. Since Cs^+, Cd^{2+}, and Te^{2-} are diamagnetic species, the magnetic (paramagnetism) contribution is expected to originate from the Ln^{3+} ions. The temperature-dependent magnetic susceptibility was fit by a least-squares method using the Curie−Weiss equation $\chi_M = C/(T - \theta)$, where χ_M is the magnetic susceptibility, C is the Curie constant, and θ is the Weiss constant. The effective magnetic moment (μ_{eff}) is calculated from the equation $\mu_{eff} = \sqrt{8\chi_M T}\mu_B$,[100] and the theoretical magnetic moment is calculated according to $\mu_{eff} = g[J(J+1)]^{1/2}$, which includes the contributions from the spin−orbital interactions.[101]

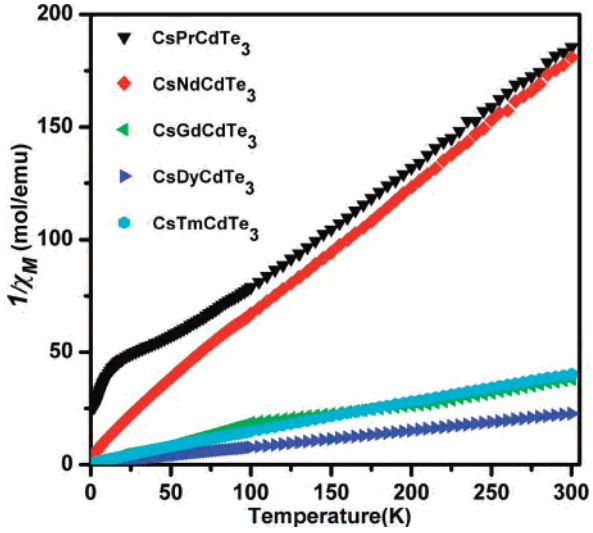

Figure 5. Plots of $1/\chi_M$ vs temperature (T) for $CsPrCdTe_3$, $CsNdCdTe_3$, $CsGdCdTe_3$, $CsDyCdTe_3$, and $CsTmCdTe_3$.

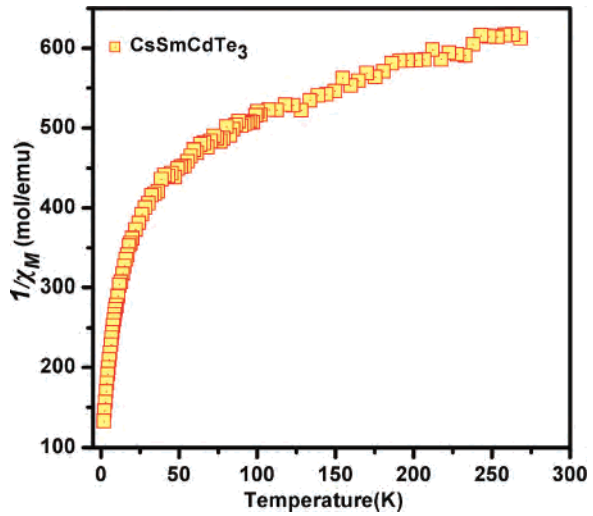

Figure 6. Plot of $1/\chi_M$ vs temperature (T) for $CsSmCdTe_3$

The plots of the reciprocal of the molar susceptibility ($1/\chi_M$) vs T are displayed in Figures 5 and 6. $CsNdCdTe_3$, $CsGdCdTe_3$, $CsDyCdTe_3$, and $CsTmCdTe_3$ obey Curie−Weiss law in the entire experimental temperature region, and $CsPrCdTe_3$ obeys the Curie−Weiss law above 50 K, whereas

(95) Huang, F. Q.; Brazis, P.; Kannewurf, C. R.; Ibers, J. A. *J. Am. Chem. Soc.* **2000**, *122*, 80.
(96) DiMasi, E.; Foran, B.; Aronson, M. C.; Lee, S. *Chem. Mater.* **1994**, *6*, 1867.
(97) Meng, F. Q.; Hughbanks, T. *Inorg. Chem.* **2001**, *40*, 2482.
(98) Chen, L.; Corbett, J. D. *Inorg. Chem.* **2004**, *43*, 3371.
(99) Quadrelli, E. A. *Inorg. Chem.* **2002**, *41*, 167.
(100) Kahn, O. *Molecular Magnetism*; VCH Publishers: New York, 1993.
(101) Van Vleck, J. H. *The Theory of Electric and Magnetic Susceptibilities*; Oxford University: Oxford, U.K., 1932; pp 226−261.

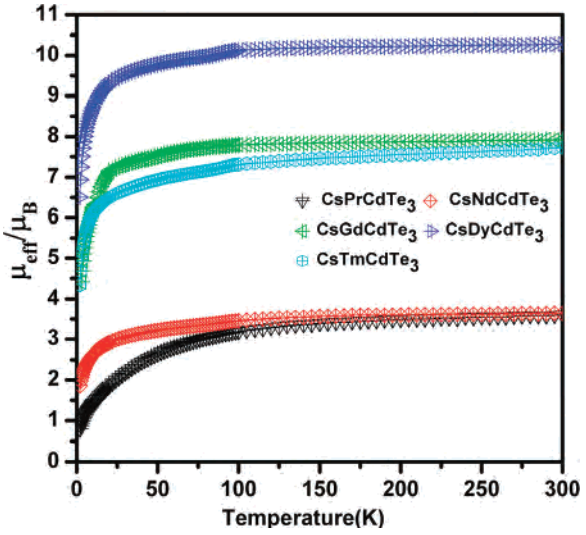

Figure 7. Plots of the experimental μ_{eff} vs temperature (T) for $CsPrCdTe_3$, $CsNdCdTe_3$, $CsGdCdTe_3$, $CsDyCdTe_3$, and $CsTmCdTe_3$.

$CsSmCdTe_3$ does not obey the Curie−Weiss law. The distinct magnetic behavior of $CsSmCdTe_3$ is typical for Sm^{3+} chalcogenides,[64,66] because the ^6H ground term for Sm^{3+} is split as a result of spin−orbit coupling, which leads to a temperature dependence of the effective moment of the 4f electrons.[100]

Linear fitting of $1/\chi_M$ with T over the whole temperature for $CsPrCdTe_3$, $CsNdCdTe_3$, $CsGdCdTe_3$, $CsDyCdTe_3$, and $CsTmCdTe_3$ indicates Curie constants (C) of 1.84, 1.18, 7.76, 13.38, and 7.50 $cm^3\ mol^{-1}$ K and Weiss constants (θ) of −44.18, −12.86, −6.79, −4.79, and −7.64 K, respectively. The effective magnetic moments (μ_{eff}) are 3.91, 3.07, 7.88, 10.35, and 7.75μ_B (Figure 7), respectively, which are comparable with the theoretical values of an isolated magnetic center per formula unit (3.58, 3.62, 7.94, 10.63, and 7.57 μ_B, respectively).[101]

The decrease in the effective magnetic moments with a decrease in temperature of $CsLnCdTe_3$ (Ln = Pr, Nd, Gd, Dy, Tm) might indicate the existence of the antiferromagnetic interactions among Ln^{3+} ions in these compounds. Note that 4f−4f antiferromagnetic interactions are much smaller than those between 3d metal ions or even between 4f and 3d ions.[102−104] Linear fittings of $1/\chi_M$ with T to the Curie−Weiss law give negative Weiss constants for all of these materials, which indicate the ligand field effect or a small degree of local antiferromagnetic ordering.

Optical Properties and Electronic Structure. Among three representative samples, $CsTmCdTe_3$ is relatively stable under ambient condition, whereas the other two, $CsNdCdTe_3$ and $CsDyCdTe_3$, turn black upon a few hours of exposure during the optical measurements. Thus, only for $CsTmCdTe_3$ were the optical properties investigated. The optical absorption spectrum performed on a single crystal of $CsTmCdTe_3$ reveals the presence of a steep fundamental absorption edge in the visible region and an optical gap of 2.01 eV (Figure 8). Such an energy gap falls in the range of a semiconductor and is consistent with the dark-red color of the compound. Polarized optical measurements on two different orientations for the crystal were investigated, and no significant differences in the measured band gaps were observed.

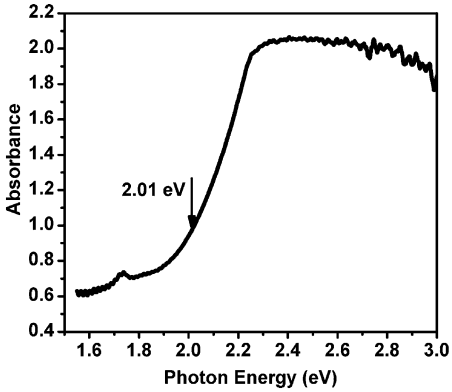

Figure 8. Optical absorption spectrum and the band gap calculation for a single crystal of $CsTmCdTe_3$.

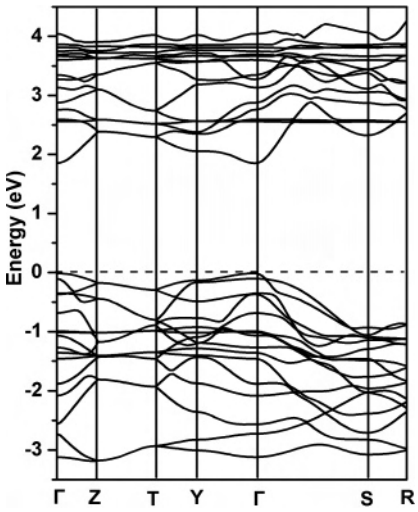

Figure 9. Band structure of $CsTmCdTe_3$ (bands are shown only between −3.5 and 4.5 eV for clarity, and the Fermi level is set at 0 eV).

The calculated band structure of $CsTmCdTe_3$ along high symmetry points of the first Brillouin zone is plotted in Figure 9. The labeled k-points are Γ (0 0 0), Z (0 0 0.5), T (0 1 0.5), Y (0 1 0), S (0.5 0.5 0), and R (0.5 0.5 0.5). The conduction band (CB) minimum (1.86 eV) and valence band (VB) maximum (0.00 eV) are both located at the Γ point. Therefore, the compound is a direct band gap semiconductor with a calculated band gap of 1.86 eV, which is comparable with the experimental value of 2.01 eV deduced from a single crystal. The discrepancy of ∼0.2 eV between the experimental and calculated band gap is not surprising, since it is well-established that one of the major inherent failures of density functional theory is that it underestimates band gaps.[105]

The total and partial densities-of-states (DOS) of $CsTmCdTe_3$ are shown in Figure 10. In principle, electron

(102) Panagiotopoulos, A.; Zafiropoulos, T. F.; Perlepes, S. P.; Bakalbassis, E.; Massonramade, I.; Kahn, O.; Terzis, A.; Raptopoulou, C. P. *Inorg. Chem.* **1995**, *34*, 4918.
(103) Andruh, M.; Ramade, I.; Codjovi, E.; Guillou, O.; Kahn, O.; Trombe, J. C. *J. Am. Chem. Soc.* **1993**, *115*, 1822.
(104) Benelli, C.; Dei, A.; Gatteschi, D.; Pardi, L. *Inorg. Chem.* **1988**, *27*, 2831.
(105) Perrin, M. A.; Wimmer, E. *Phys. Rev. B* **1996**, *54*, 2428.

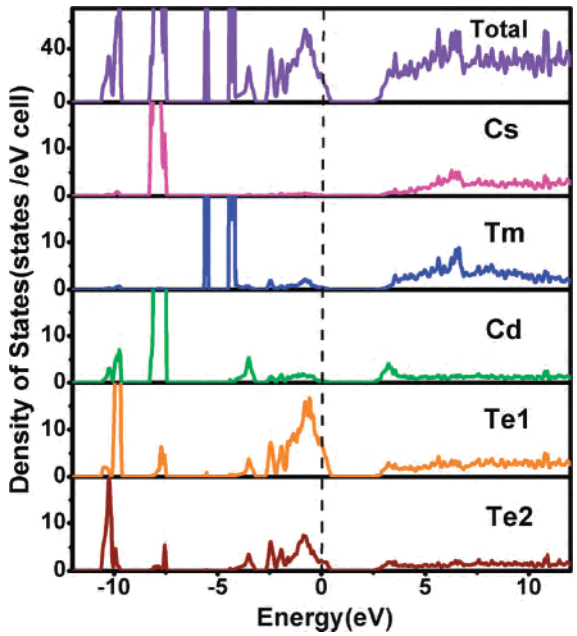

Figure 10. Total and partial DOS of $CsTmCdTe_3$.

correlation is treated in a more accurate way within the GGA than within LDA. An alternative approach, GGA(PBE)+U, allows us to get a better agreement between the calculated and observed electronic properties.[88,89] So the GGA(PBE)+U approach to the DOS and the band structure is very reliable on account of the U presence. The calculations indicate that the VB maximum near the Fermi level (0.0 eV) is mostly made up of Te(5p) states mixed with a small amount of the Tm(6s and 5d) and Cd(5s and 5p) states, whereas the CB minimum has most of its contributions from Te(5s and 5p) states, Tm(5d) states, and Cd(5s and 5p) states and minor contributions from Cs(6s) states. As shown in Figure 10, the shape of Te(5p) is similar to those of the Cs(5p), Tm(6s and 5d), and Cd(5s and 5p) states, but their density of states are different from −3.0 eV up to the Fermi level, which indicates the strong covalent interactions between Te and Tm/Cd atoms and typical ionic interactions between Te and Cs atoms. As a result, the two-dimensional $_\infty^2[LnCdTe_3^-]$ anionic framework may play an important role in the electronic properties of the compound.

Because the sequence of energy levels of p orbitals is 4p(Se) < 5p(Te), the band gaps of $CsLnCdTe_3$ compounds should be smaller than those of the $CsLnCdSe_3$ analogues. This is demonstrated by both the experimental measurements and the theoretical studies in the present paper. For example, $Eg_{(exp)} = 2.01$ eV for $CsTmCdTe_3$ vs 2.54 eV for $CsYCdSe_3$ measured from (001).[66] A similar decrease in the band gap ($\Delta Eg_{(exp)} = 0.11$ eV) has also been observed when Zn in $CsLnMTe_3$ has been replaced by Cd, $Eg_{(exp)} = 2.12$ eV for $CsTbZnTe_3$ analogues.[74] Since the VBs of $CsLn(Cd/Zn)Te_3$ compounds are both primarily Te(5p) in character, the differences in band gaps are a result of the different constituents of CBs, Cd(5s and 5p) in the $CsLnCdTe_3$ compounds and Zn(4s and 4p) in the $CsLnZnTe_3$ compounds.[74] Similarly, the band gap of CdSe is smaller than that of the ZnSe.[66]

Concluding Remarks

In summary, 11 new quaternary rare-earth layered chalcogenides, $CsLnCdTe_3$ (Ln = La, Pr, Nd, Sm, Gd−Tm, and Lu), have been prepared by the reactive flux method at high temperature. With the successful involvement of both cesium and lanthanide, the structure and band gap of binary CdTe are successfully tailored and tuned. The single-crystal optical energy band gap of the representative compound $CsTmCdTe_3$ (2.01 eV) exhibits a noticeable blue shift compared with that of bulk CdTe (1.44 eV), which is attributed to the reduction of the structural dimensionality. The theoretical calculations on the electronic structure of $CsTmCdTe_3$ confirm the important role that Cs and Tm atoms play to influence the optical properties. The magnetic properties observed in these materials are a result of the involvement of the magnetic Ln^{3+} species. These $CsLnCdTe_3$ compounds show interesting properties and may potentially be useful as new optoelectronic materials.

Acknowledgment. This research was supported by the National Natural Science Foundation of China under Projects (20401014, 20401013, 20521101, 20773130), the State Key Laboratory Science Foundation (070023 and 050097), NSF of Fujian Province (2004HZ01-1, 2005HZ01-1, 2006J0271), and the "Key Project from CAS" (KJCX2-YW-H01). G.H.C. and R.P.V.D. thank the MRSEC program of the National Science Foundation (DMR-0520513) at the Materials Research Center of Northwestern University for funding. We thank Prof. James A. Ibers for kindly allowing us to use his goniometer head for the single-crystal absorption measurements.

Supporting Information Available: X-ray data in CIF format for compounds. This material is available free of charge via the Internet at http://pubs.acs.org.

IC7016402